Available online at www.sciencedirect.com
SCIENCE DIRECT®
Journal of Crystal Growth 252 (2003) 413–423
JOURNAL OF CRYSTAL GROWTH
www.elsevier.com/locate/jcrysgro

Effects of a rotating magnetic field on the thermocapillary instability in the floating zone process

J.S. Walker[a,*], L.Martin Witkowski[b], B.C. Houchens[a]

[a] *Department of Mechanical and Industrial Engineering, University of Illinois, 1206 West Green Street, Urbana, IL 61801, USA*
[b] *LIMSI, BP133, F91403 Orsay Cedex, France*

Received 28 October 2002; accepted 24 December 2002
Communicated by D.T.J. Hurle

Abstract

This paper presents a linear stability analysis for the thermocapillary convection in the floating zone process with a rotating magnetic field (RMF). For every case with a RMF, there is a transition from a steady, axisymmetric flow to a periodic, nonaxisymmetric flow at a critical value of *Re*, the Reynolds number for the thermocapillary convection. As *Tm*, the magnetic Taylor number for the RMF, is increased from zero, the critical value of *Re* first decreases to a minimum and then increases as the azimuthal flow velocity becomes strong enough to damp the radial and axial flow velocities. Critical modes for some values of *Tm* involve azimuthal wave velocities which are greater than the maximum azimuthal flow velocity, while critical modes for other values of *Tm* could be nonaxisymmetric patterns which are convected by the azimuthal flow velocity. Results are presented for three values of the Prandtl number.

PACS: 47.20.Dr; 47.62.+q; 47.65.+a; 81.05.Cy

Keywords: A1. Computer simulation; A1. Magnetic fields; A2. Floating zone technique

1. Introduction

For several bulk-growth processes, the quality of semiconductor crystals is improved by the application of a rotating magnetic field (RMF) to the melt during growth. An RMF is produced by connecting a multiphase AC power source to inductors at equally spaced azimuthal positions around an axisymmetric melt zone. For most crystal growth processes, the RMF is a spatially uniform transverse magnetic field, which rotates at a constant angular velocity ω around the vertical centerline of the melt. For the magnetic field strengths and frequencies used in practice, the RMF produces a steady, axisymmetric, azimuthal body force on the melt. This body force drives an azimuthal melt velocity v_θ which may stabilize the natural convection through the Taylor-column effect. In addition the axial variation of the centrifugal force due to v_θ drives a meridional melt flow with radial and axial melt velocities v_r, v_z and this forced meridional circulation can lead to a

*Corresponding author. Tel.: +1-217-333-7979; fax: +1-217-244-6534.
E-mail address: jswalker@uiuc.edu (J.S. Walker).

0022-0248/03/$ - see front matter
doi:10.1016/S0022-0248(03)00834-0

more planar crystal–melt interface and to more uniform axial and radial dopant distributions in the crystals. Dold and Benz [1] recently presented an excellent review of the pre-1999 research on RMFs in crystal growth processes.

In the floating zone (FZ) process with optical heating, a short, nearly cylindrical melt zone is held by surface tension between the melting bottom of a cylindrical feed rod and the solidifying top of a coaxial, cylindrical single crystal. Two advantages of the FZ process are the absence of contamination from a crucible and the absence of defects due to the contact forces between the crystal and an ampoule. Since the surface tension of most molten semiconductors decreases as the temperature is increased, the melt motion in the FZ process includes a thermocapillary convection with axial free-surface flows from the hottest circumference toward the peripheries of the feed rod and crystal, and with the circulations completed by axial flows toward the middle plane in the interior of the melt. Unfortunately, the thermocapillary convection has a hydrodynamic instability for a free-surface temperature difference which is one or two orders of magnitude smaller than the temperature difference required for crystal growth. This instability leads to an unsteady, nonaxisymmetric melt motion, which produces undesirable striations in the crystal.

Recently, Dold et al. [2] used the FZ process with an RMF to grow silicon crystals with diameters of 8–14 mm. As the strength of the 50 Hz RMF was increased from zero to 7.5 mT, the difference between the maximum and minimum dopant concentrations in the striations and the average distance between adjacent dopant maxima both decreased dramatically. Both improvements are due to the increase in frequency of the unsteady melt motion. For the stronger RMFs, the frequency of the unsteady melt motion, which was inferred from the striation spacing and the growth rate, appeared to correlate with the frequency of the azimuthal circulation driven by the RMF. While the RMF did not eliminate the thermocapillary instability, it greatly reduced its deleterious effects. Both experimental measurements and numerical predictions indicated that the deviation from axisymmetry in the melt motion was reduced by the RMF, but that a nonaxisymmetric, periodic melt motion persisted. Dold et al. [2] indicated that this residual deviation from axisymmetry may have occurred because the thermocapillary convection was still unstable in spite of the RMF or may have occurred because the centerlines of the melt and magnet were not perfectly aligned. The results presented here show that the values of Re, the Reynolds number for the thermocapillary convection, in their experiments was still far above the critical value of Re for transition from steady, axisymmetric flow to unsteady, nonaxisymmetric flow. Therefore the RMF in their experiments did not eliminate the thermocapillary instability.

This paper presents a linear stability analysis for the thermocapillary convection in a melt zone with a cylindrical free surface and with the same solidification temperature at the two planar liquid–solid interfaces. There is an axisymmetric heat flux into the free surface which varies parabolically from a maximum $q_{\max}$ at the plane midway between the liquid–solid interfaces to zero at the peripheries of these interfaces. We neglect the sagging of the free surface and the buoyant convection, which are both associated with gravity. Many researchers have treated the thermocapillary instability in the half-zone problem without an RMF [3–9]. The half-zone problem has the same geometry, but there is no heat flux into the free surface, and the liquid–solid interfaces are at different temperatures. The half-zone problem is supposed to model half the melt zone of the actual FZ process, and the hotter liquid–solid interface is supposed to represent the middle plane of the actual FZ process. The previous results for the half-zone problem without an RMF provide comparisons which aid the physical interpretation of our results. In addition we modified our numerical model to match the boundary conditions of the half-zone problem in order to validate our numerical accuracy. For example, for an axial half-zone length equal to its radius and for a Prandtl number $Pr = 0.02$, our code gives a critical value of $Re = 2059$, while Chen et al. [8] obtained a value of 2054 and Wanshura et al. [5] obtained a value of 2062.

For the present problem with the same temperature at the two liquid–solid interfaces and with a heat flux into the free surface, Kasperski et al. [10] treated the transition from a steady, axisymmetric flow to a periodic, axisymmetric flow without an RMF. However, the critical value of Re for this transition to a periodic, axisymmetric flow is far above that for the transition to a steady, nonaxisymmetric flow without an RMF.

This paper only treats the first instability involving a transition from a steady axisymmetric flow to a periodic nonaxisymmetric flow. Without an RMF, there is a series of instabilities. The first instability involves transition from a steady axisymmetric flow to a steady nonaxisymmetric flow. The second instability involves transition from the steady nonaxisymmetric flow to a periodic nonaxisymmetric flow. Additional instabilities eventually lead to turbulent flow. With any RMF, the first instability leads to a periodic nonaxisymmetric flow. There are certainly other instabilities at higher values of Re, but the nature of these instabilities is clearly different from those without an RMF.

2. Problem formulation

For the RMF strengths and frequencies used in the experiments of Dold et al. [2] and in virtually all crystal growth processes with RMF's, the effects of the melt motion on the magnetic field and electric current are negligible. The frequencies and magnetic flux densities for which the RMF body force is independent of the melt motion and is steady, axisymmetric and purely azimuthal are defined by Martin Witkowski et al. [11]. Therefore this is an ordinary hydrodynamic flow with a known, steady, axisymmetric, azimuthal body force due to the RMF, rather than a magnetohydrodynamic flow with an intrinsic coupling between the hydrodynamic and electromagnetic variables.

We assume that all the thermophysical properties of the melt are uniform and constant, except the surface tension, which decreases linearly with increasing temperature. We use cylindrical coordinates (r, θ, z) with the z-axis along the centerline of the cylindrical melt zone, with the origin at the center of the melt, and with the unit vectors $(\hat{\mathbf{r}}, \hat{\theta}, \hat{\mathbf{z}})$. We normalize r and z with R, the radius of the melt zone, and we assume that the axial distance between the two liquid–solid interfaces is $2R$, because the melt zone in the actual FZ process does not deviate much from this aspect ratio.

The dimensionless governing equations are

$$\frac{\partial \mathbf{v}}{\partial t} + (\mathbf{v}\bullet\nabla)\mathbf{v} = -\nabla p + Tmf_\theta\hat{\theta} + \nabla^2\mathbf{v}, \tag{1a}$$

$$\nabla\bullet\mathbf{v} = 0, \tag{1b}$$

$$\frac{\partial T}{\partial t} + \mathbf{v}\bullet\nabla T = Pr^{-1}\nabla^2 T. \tag{1c}$$

The dimensionless variables t, $\mathbf{v}$, p and T are time, the melt velocity, the melt pressure and the deviation of the melt temperature from the solidification temperature, each normalized by $R^2/\nu, \nu/R, \rho\nu^2/R^2$ and $(\Delta T)_c$, respectively. The dimensionless parameters here are the magnetic Taylor number $Tm = \sigma\omega B^2R^4/2\rho\nu^2$, and the Prandtl number, $Pr = \nu/\kappa$, where ν, ρ, σ and κ are the kinematic viscosity, density, electrical conductivity and thermal diffusivity of the melt, while $(\Delta T)_c$ is a characteristic temperature difference, and B is the magnetic flux density of the RMF. Assuming that the electric currents flowing through the crystal and feed rod are negligible, the dimensionless azimuthal body force due to the RMF [11] is

$$f_\theta = r - 2\sum_{N=1}^{\infty}\frac{J_1(\lambda_N r)\cos h(\lambda_N z)}{(\lambda_N^2 - 1)J_1(\lambda_N)\cos h(\lambda_N)}, \tag{2}$$

where J_k is the Bessel function of the first kind and kth order, while λ_N are the roots of $\lambda_N J_0(\lambda_N) - J_1(\lambda_N) = 0$.

We use $(\Delta T)_c = Rq_{max}/k$ for the characteristic temperature difference, where k is the thermal conductivity of the melt. Therefore the boundary conditions at $r = 1$ are

$$v_r = 0, \quad \frac{\partial v_\theta}{\partial r} - v_\theta + Re\frac{\partial T}{\partial \theta} = 0, \tag{3a, b}$$

$$\frac{\partial v_z}{\partial r} + Re\frac{\partial T}{\partial z} = 0, \quad \frac{\partial T}{\partial r} = 1 - z^2, \tag{3c, d}$$

where the Reynolds number, $Re = (-d\gamma/dT)(\Delta T)_c R/\rho\nu^2$, and $d\gamma/dT$ is the constant,

negative derivative of the surface tension with respect to temperature. The boundary conditions at $z = \pm 1$ are $\mathbf{v} = T = 0$.

For each variable v_r, v_θ, v_z, p, and T, we introduce the form

$$v_r = v_{r0}(r,z) + \varepsilon \mathrm{Real}\,[v_{r1}(r,z)\exp(\lambda t - \mathrm{i}m\theta)]. \quad (4)$$

The subscript 0 denotes the variables for the steady, axisymmetric base flow, the subscript 1 denotes the complex modal functions, such as $v_{r1R} + \mathrm{i}v_{r1I}$, for the small, $O(\varepsilon)$ perturbation in the linear stability analysis, $\lambda = \lambda_R + \mathrm{i}\lambda_I$ is the complex eigenvalue, and m is the real, integer azimuthal wave number.

For the base flow, we introduce the stream function $\psi_0(r,z)$, where

$$v_{r0} = \frac{1}{r}\frac{\partial \psi_0}{\partial z}, \quad v_{z0} = -\frac{1}{r}\frac{\partial \psi_0}{\partial r}. \quad (5a, b)$$

We eliminate p_0 by cross-differentiating the r and z components of the momentum Eq. (1a) for the steady, axisymmetric base flow. Since $v_{\theta 0}$ and T_0 are even functions of z, while ψ_0 is an odd function of z, we need only treat $0 < z < 1$ for the base flow with symmetry conditions at $z = 0$. We represent each base-flow variable by a sum of Chebyshev polynomials in r and z, and we insure that the representation for each variable has the correct Taylor series in r, e.g., the Taylor series of ψ_0 has only even powers of r, beginning with r^2. We apply the governing equations and boundary conditions at the Gauss–Lobatto collocation points. We solve the nonlinear, algebraic equations for the coefficients in the Chebyshev-polynomial representations using the Newton–Raphson method.

Since the base flow is symmetric in z, we need only treat $0 < z < 1$ for the small perturbations as long as we consider both symmetric and antisymmetric modes. For a symmetric mode, $v_{r1}, v_{\theta 1}, p_1$ and T_1 are even functions of z, while v_{z1} is an odd function of z, thus matching the symmetry of the base flow. For an antisymmetric mode, $v_{r1}, v_{\theta 1}, p_1$ and T_1 are odd functions of z, while v_{z1} is an even function of z. The small-perturbation boundary value problem for $m = 0$ is different and simpler compared to that for $m \geqslant 1$, so that we treat four perturbation cases: namely symmetric and antisymmetric modes with $m = 0$ and $m \geqslant 1$. We represent each perturbation variable as a sum of Chebyshev polynomials in r and z, and again we insure that each representation has the correct Taylor series expansion, e.g., the Taylor series for v_{r1} for $m \geqslant 1$ has the powers $r^{(m-1)}, r^{(m+1)}, r^{(m+3)}, \ldots$ The linear perturbation equations and boundary conditions are applied at the Gauss–Lobatto collocation points to obtain a linear, matrix eigenvalue problem. The eigenvalues are obtained with subroutines from the EISPACK library of FORTRAN codes [12].

For each set of values for Pr, Tm and Re, we first used the Newton–Raphson iteration to find the steady, axisymmetric base flow, and then we used the EISPACK subroutines to find the eigenvalues for the symmetric and antisymmetric perturbation modes for $m = 0$–4. For each set of values for Pr and Tm, we increased Re until one eigenvalue for one mode had $\lambda_R = 0$, while all the other eigenvalues for this mode and for all the other modes had $\lambda_R < 0$. We normalized the complex modal functions for the critical mode by setting the first coefficient in the Chebyshev-polynomial representation for v_{r1} equal to one. This normalization scales the modal functions and eliminates the arbitrary rotation in θ.

3. Results

We present results for $Pr = 0.001$, 0.02 and 0.04 and for $Tm = 0$–8000. For every case considered here, the first perturbation to become unstable is an antisymmetric mode with $m = 1$ or 2. The critical values of the Reynolds number, Re_{cr}, for all three values of Pr are presented in Fig. 1a for $0 < Tm < 1400$ and in Fig. 1b for $1000 < Tm < 8000$. For $Tm = 0$, $m = 2$ and $\lambda_\mathrm{I} = 0$ for the critical mode, while $Re_{\mathrm{cr}} = 1205$, 1548 and 2440 for $Pr =$ 0.001, 0.02 and 0.04, respectively. For the half-zone problem, Chen et al. [8] obtained $Re_{\mathrm{cr}} =$ 1793, 2054 and 2704 for $Pr = 0.001$, 0.02 and 0.04, respectively, also for $m = 2$ and $\lambda_\mathrm{I} = 0$. The half-zone problem corresponds to our problem for $0 < z < 1$ with a rigid wall with $T = 1$ at $z = 0$ and with $\partial T/\partial r = 0$ at $r = 1$. The first reason that Re_{cr} for the half-zone problem is higher than that for

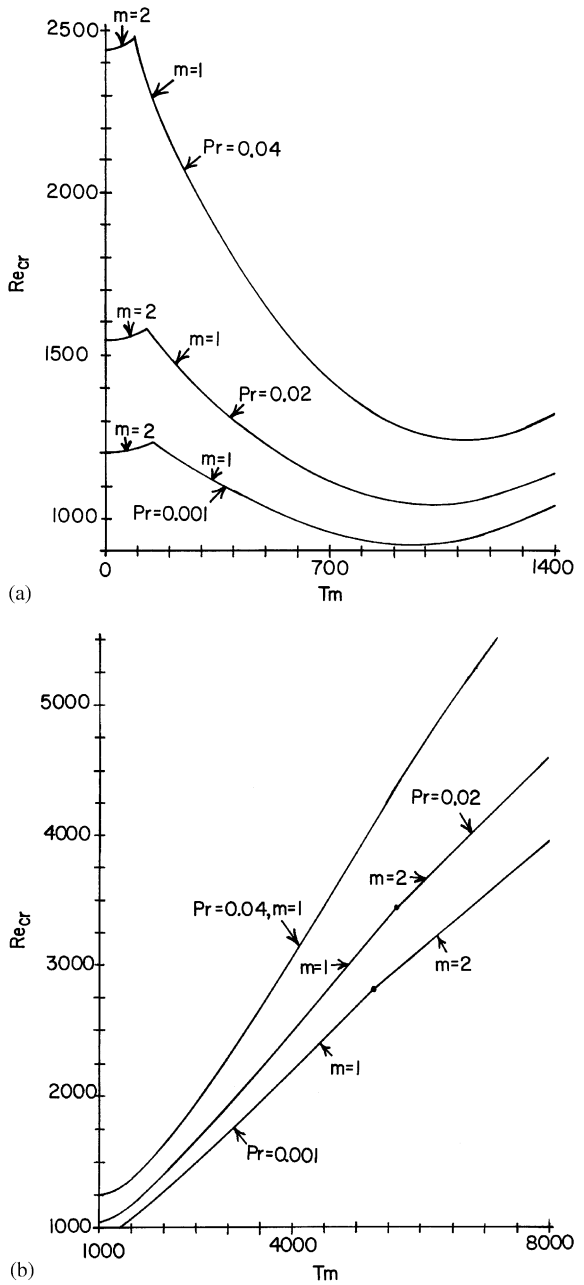

Fig. 1. Re_{cr} versus Tm for $Pr = 0.001$, 0.02 and 0.04: (a) $0 < Tm < 1400$; (b) $1000 < Tm < 8000$.

the present FZ problem is that the perturbation in the half-zone problem with $v_{z1} = 0$ at $z = 0$ corresponds roughly to a symmetric mode in our problem, and our results show that the antisymmetric mode with $m = 2$ becomes unstable at a lower value of Re than any symmetric mode. However, the Re_{cr} for the symmetric mode with $m = 2$ is less than 100 more that the Re_{cr} for the antisymmetric mode with $m = 2$ for $Tm = 0$ and for all three values of Pr. Therefore this first reason only explains part of the difference. A second difference is that our Re is based on q_{max}, while the half-zone Re is based on the free-surface temperature difference. We can correct for this difference by multiplying each of our values of Re_{cr} times the maximum dimensionless temperature in the base flow, which always occurs at $r = 1$ and $z = 0$. This correction gives $Re_{cr}T_{0max} = 1279$, 1549 and 2147 for $Pr = 0.001$, 0.02 and 0.04, respectively. This correction increases the difference from the half-zone results of Chen et al. [8] for $Pr = 0.04$. A third reason for the differences is that the half-zone problem has a rigid wall with a no-slip condition at $z = 0$, while the symmetric modes for the FZ problem have a traction-free condition at $z = 0$, so that there is more stabilizing viscous dissipation in the half-zone problem. A fourth reason for the differences is that, for the same free-surface temperature difference, the half-zone problem has a nearly uniform value of $\partial T_0/\partial z$ over the free surface for these small values of Pr, while the FZ problem involves a decrease of $\partial T_0/\partial z$ from zero at $z = 0$ to roughly double that in the half-zone problem at $z = 1$. The larger maximum free-surface temperature gradient appears to lead to instability at a lower value of Re_{cr}.

As Tm is increased from zero, Re_{cr} increases slightly until there is a switch from the $m = 2$ antisymmetric mode to the $m = 1$ antisymmetric mode. This switch occurs at $Tm = 147$, $Re_{cr} = 1234$ for $Pr = 0.001$, at $Tm = 131$, $Re_{cr} = 1580$ for $Pr = 0.02$, and at $Tm = 95$, $Re_{cr} = 2482$ for $Pr = 0.04$. As Tm is increased from this switch to the $m = 1$ mode, Re_{cr} decreases to a minimum of 918 at $Tm = 959$ for $Pr = 0.001$, to a minimum of 1038 at $Tm = 1012$ for $Pr = 0.02$, and to a minimum of 1241 at $Tm = 1128$ for $Pr = 0.04$. As Tm is increased from this minimum, Re_{cr} increases monotonically, as shown in Fig. 1b. There is switch back from the $m = 1$ antisymmetric mode to the $m = 2$ antisymmetric mode at $Tm = 5261$, $Re_{cr} = 2811$ for $Pr = 0.001$ and at $Tm = 5620$,

$Re_{cr} = 3429$ for $Pr = 0.02$. For $Pr = 0.04$, it appears that this modal switch occurs close to $Tm = 8000$.

The critical perturbation involves a spatially fixed pattern which rotates in the θ direction with the angular phase velocity (λ_I/m). This disturbance rotation may represent merely convection with some mean base-flow angular velocity or it may represent wave propagation relative to the base-flow azimuthal motion, either in the same azimuthal direction or in the opposite direction. The angular phase velocity (λ_I/m) for the critical mode and the maximum base-flow angular velocity $(v_{\theta 0}/r)_{max}$ are plotted in Fig. 2a for $Pr = 0.02$ and $0 < Tm < 600$. The corresponding plots for $Pr = 0.001$ and 0.04 are very similar. For the $m = 2$ mode, which is the first instability for $0 < Tm < 131$, the angular phase velocity is slightly more than half the maximum base-flow angular velocity. For $Tm = 0$, the critical instability involves an $m = 2$ pattern which does not rotate, i.e., $\lambda_I = 0$ [8], and we conclude that for $Tm < 131$, the instability involves essentially the same pattern being convected with some average of the base-flow angular velocity. For the $m = 1$ mode for $Tm > 131$, the angular phase velocity is always larger than the maximum base-flow angular velocity, so that this mode is definitely propagating relative to the base-flow angular velocity and in the same direction. At $Tm = 131$, the angular phase velocity for $m = 1$ is more than twice the maximum base-flow angular velocity, so that the instability is racing ahead of the azimuthal base flow. The difference, $(\lambda_I/m) - (v_{\theta 0}/r)_{max}$, decreases from 15.0 at $Tm = 131$ to a minimum of 7.4 near $Tm = 1000$ and then increases, asymptoting to roughly 17.0 for $Tm > 3000$. Clearly the minimum of this difference correlates with the minimum of Re_{cr} in Fig. 1a. The values of (λ_I/m) and $(v_{\theta 0}/r)_{max}$ for $3000 < Tm < 8000$ are presented in Fig. 2b. Again the $m = 1$ mode for $Tm < 5620$ is clearly propagating in the $+\theta$ direction with a phase velocity which is larger than the maximum base-flow angular velocity. For the $m = 2$ mode for $Tm > 5620$, (λ_I/m) is less than $(v_{\theta 0}/r)_{max}$. For the larger values of Tm, part of the melt near the origin has a rigid-body rotation, as illustrated by the contours of $v_{\theta 0}$ for $Pr = 0.02$, $Tm = 8000$ and

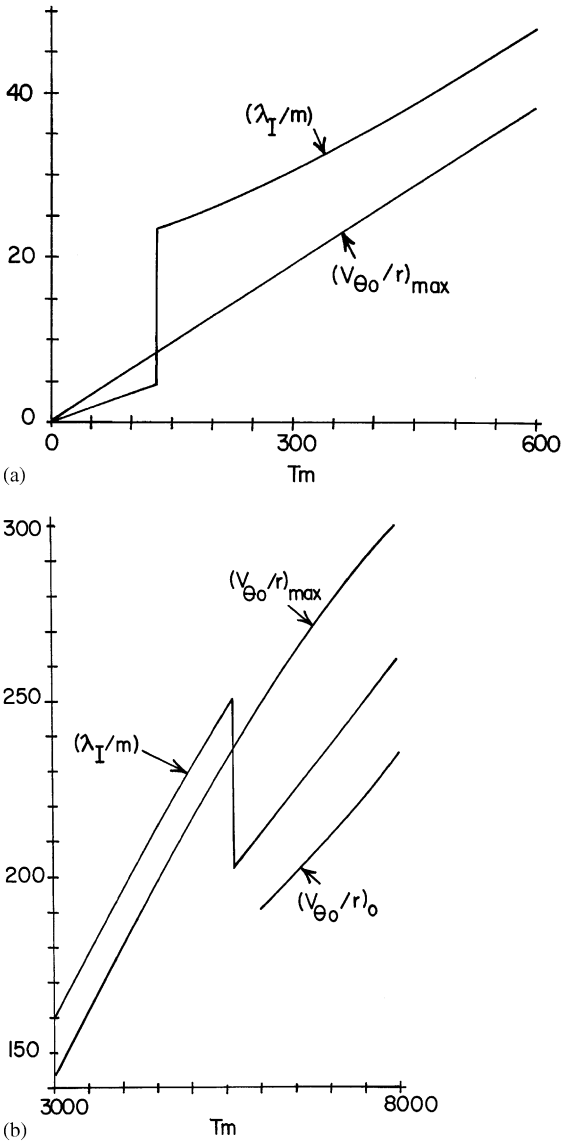

Fig. 2. The angular phase velocity (λ_I/m) for the critical mode and the maximum base-flow angular velocity $(v_{\theta 0}/r)_{max}$ versus Tm for $Pr = 0.02$: (a) $0 < Tm < 600$; (b) $3000 < Tm < 8000$. The base-flow angular velocity at the origin is also plotted for $Tm > 6000$.

$Re_{cr} = 4593$ in Fig. 3. This region of rigid-body rotation in the base flow only emerges for $Tm > 1500$. The angular velocity for this rigid-body rotation is plotted as $(v_{\theta 0}/r)_0$ in Fig. 2b. As z is increased from 0 to 1, the base-flow angular velocity increases from roughly $(v_{\theta 0}/r)_0$ at $z = 0$

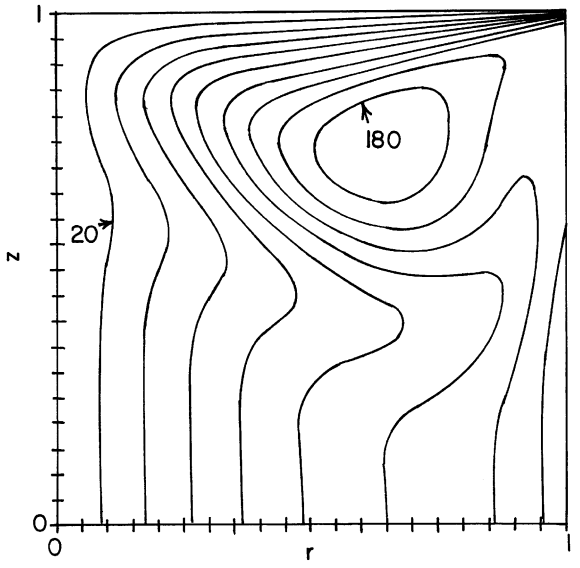

Fig. 3. Contours of $v_{\theta 0}$ for $Pr = 0.02$, $Tm = 8000$ and $Re_{cr} = 4593$. $v_{\theta 0} = 20n$, for $n = 1$–9.

to roughly $(v_{\theta 0}/r)_{max}$ near $z = 0.75$ and then decreases to zero at $z = 1$. The relationship between the curves in Fig. 2b appears to indicate that the critical $m = 2$ mode for $Tm > 5620$ does not involve any wave propagation and is simply being convected with some mean base-flow angular velocity.

For $Tm = 0$, the critical antisymmetric mode with $m = 2$ and $\lambda_I = 0$ involves a stationary pattern where v_{z1} at the free surface is positive at $\theta = 0, \pi$ and is negative at $\theta = \pm\pi/2$. For $z > 0$, the associated convective heat transfer makes the free-surface T_1 positive at $\theta = 0, \pi$ and negative at $\theta = \pm\pi/2$. Most of the upward and downward perturbation flows near the free surface complete their circuit with appropriate values of $v_{\theta 1}$ near the free surface, but part of these upward and downward flows circulate in $\theta =$ constant planes with opposite signs for v_{z1} near $r = 0$. This perturbation pattern is very similar to that described by Chen et al. [8] for the half-zone problem. As Tm is increased from 0 to the switch from $m = 2$ to 1, this pattern is simply convected in the $+\theta$ direction with the base-flow angular velocity, and the angular phase velocity increases nearly linearly with Tm.

The wave propagation of the $m = 1$ mode in the $+\theta$ direction involves the interaction of the centrifugal force in the radial momentum equation and the radial transport of angular momentum in the azimuthal momentum equation. The key terms in the perturbation equations are

$$\frac{\partial v_{r1}}{\partial t} = \frac{2}{r} v_{\theta 1} v_{\theta 0} + \cdots, \tag{6a}$$

$$\frac{\partial v_{\theta 1}}{\partial t} = -\frac{v_{r1}}{r}\frac{\partial}{\partial r}(r v_{\theta 0}) + \cdots, \tag{6b}$$

where λ has been replaced by $\partial/\partial t$ for this discussion. The value of $v_{\theta 0}$ is positive everywhere and the value of $\partial(rv_{\theta 0})/\partial r$ has a local maximum near the global maximum of $v_{\theta 0}$. For example, for the values plotted in Fig. 3, the global maximum value of $v_{\theta 0}$ occurs at $r = 0.65$, $z = 0.75$, and the nearby local maximum value of $\partial(rv_{\theta 0})/\partial r$ occurs at $r = 0.5$, $z = 0.75$. We consider the time history of $v_{\theta 1}$ and v_{r1} at a fixed point in space, beginning with $v_{\theta 1} > 0$ and $v_{r1} = 0$. Eq. (6a) indicates that v_{r1} will increase from zero to positive values, so that Eq. (6b) indicates that $v_{\theta 1}$ will decrease from its initial positive value. After a quarter period, $v_{\theta 1}$ has decreased to zero and v_{r1} has increased to its maximum positive value. Eq. (6b) indicates that $v_{\theta 1}$ will now decrease from zero to negative values, so that Eq. (6a) indicates that v_{r1} will decrease from its maximum value. After a half period, v_{r1} has decreased to zero and $v_{\theta 1}$ has reached its minimum negative value. Eq. (6a) indicates that v_{r1} will now decrease from zero to negative values, so that Eq. (6b) indicates that $v_{\theta 1}$ will increase from its negative value. After three-quarters of a period, $v_{\theta 1}$ has increased to zero and v_{r1} has reached its minimum negative value. Eq. (6b) indicates that $v_{\theta 1}$will now increase from zero to positive values, so that Eq. (6a) indicates that v_{r1} will increase from its negative value. After a full period, $v_{\theta 1}$ has increased to its maximum positive value and v_{r1} has returned to zero. Of course, the other terms in the perturbation equations will create some phase shift from this simplified description based only on the key terms in Eq. (6). For $Pr = 0.001$, $Tm = 1000$ and $Re_{cr} = 919$, the values of $v_{\theta 1}$ and v_{r1} at $r = 0.5$, $\theta = 0$ and $z = 0.6$ are plotted as functions of $\lambda_I t$ in Fig. 4. This point in the melt was chosen because it is midway between the points where $v_{\theta 0}$

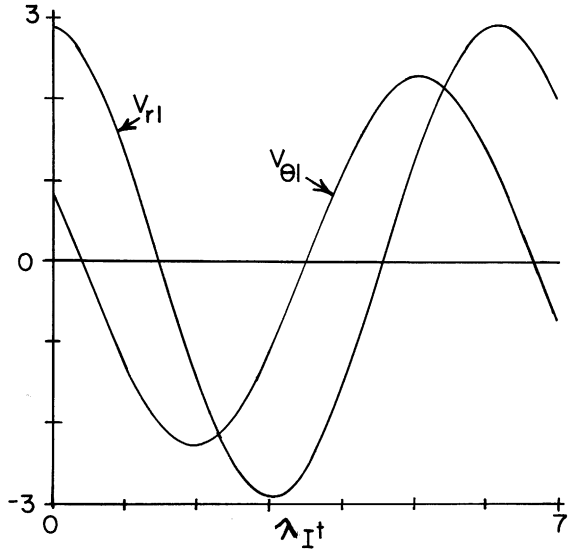

Fig. 4. Values of $v_{\theta 1}$andv_{r1} at $r = 0.5$, $\theta = 0$ and $z = 0.6$ for $Pr = 0.001$, $Tm = 1000$ and $Re_{cr} = 919$.

and $\partial(rv_{\theta 0})/\partial r$ have their maxima. The maximum of $v_{\theta 1}$ occurs at $\Delta(\lambda_I t) = 1.08$ before the maximum of v_{r1}, while this phase shift would be $\pi/2 = 1.57$ for our simple model. Eq. (6) would give

$$\lambda_I = \left[2\left(\frac{v_{\theta 0}}{r}\right)\left(\frac{v_{\theta 0}}{r} + \frac{\partial v_{\theta 0}}{\partial r}\right)\right]^{1/2}. \quad (7)$$

While this is a simplistic model, Eq. (7) provides some physical insights into the reason that $\lambda_I > (v_{\theta 0}/r)_{max}$ for the propagating $m = 1$ mode.

For $Tm = 0$, $v_{\theta 0} = 0$ and Eq. (6) indicate that the propagating $m = 1$ mode does not exist, i.e., its $Re_{cr} = \infty$. As Tm is increased from zero and the RMF produces a small azimuthal base-flow velocity, the Re_{cr} for the propagating $m = 1$ mode decreases rapidly from infinity and crosses the Re_{cr} for the convected $m = 2$ mode at $Tm = 95$–147 for our three values of Pr. For $Tm = 200$–500, the RMF adds angular momentum to the base flow, and this angular momentum is convected by the meridional thermocapillary convection, but the base-flow centrifugal force is too small to have any effect on the meridional thermocapillary convection. For these small values of Tm, $v_{\theta 0max}$ is much smaller than v_{r0max}, so that $v_{r0}\partial(rv_{\theta 0})/\partial r$ is important in the azimuthal base-flow momentum equation, but $v_{\theta 0}^2/r$ is negligible in the radial base-flow momentum equation. On the other hand, these two terms are equally important in the perturbation momentum equations and are responsible for the propagating $m = 1$ instability because $v_{\theta 1}$ and v_{r1} are comparable in magnitude, as shown in Fig. 4. The addition of a small azimuthal velocity to a strong meridional convection feeds the propagating $m = 1$ instability and leads to the decrease of Re_{cr} as Tm is first increased after the switch from $m = 2$ to 1. The difference in magnitudes of v_{r0} and $v_{\theta 0}$ is illustrated by the fact that $\psi_{0max} = 13.1$ and $v_{\theta 0max} = 3.77$ for $Tm = 100$ and the $Re_{cr} = 1567$ for $Pr = 0.02$, while $\psi_{0max} = 0.329$ and $v_{\theta 0max} = 22.0$ for $Tm = 100$ and $Re = 0$, i.e., with the RMF, but without the thermocapillary convection. As Tm increases from 500, $v_{\theta 0}$ becomes large enough that the associated centrifugal force begins to modify the thermocapillary convection. Compared to the thermocapillary convection for the same Re and for $Tm = 0$, the meridional convection for $Tm > 500$ extends a shorter radial distance from the free surface, is shifted toward $z = 1$ and has a smaller value of ψ_{0max}. These modifications arise from the Taylor-column effect: radially inward flow tends to conserve angular momentum $rv_{\theta 0}$, so that its $v_{\theta 0}$ increases, and the associated increase in the radial centrifugal force opposes the radially inward flow. The reduction of the radial extent of the thermocapillary convection leads to its concentration near $z = 1$ where $-\partial T_0/\partial z$ at the free surface is maximum. The modification of the meridional convection by the centrifugal force is illustrated by the base-flow streamlines for $Tm = 8000$, $Re_{cr} = 4593$ and $Pr = 0.02$ in Fig. 5, corresponding to the contours of $v_{\theta 0}$ in Fig. 3. The stabilizing effect of the growing base-flow centrifugal force leads first to the minimum of Re_{cr} near $Tm = 1000$ and then to the increase of Re_{cr} for larger values of Tm. As Tm is increased from zero, the rate of increase of Re_{cr} for the convected $m = 2$ mode changes from a parabolic variation near $Tm = 0$ to a linear variation for $Tm > 6000$, while the Re_{cr} for the propagating $m = 1$ mode first decreases, reaches a minimum as the base-flow centrifugal force begins to modify the meridional thermocapillary convection, and then increases rapidly as the modification of the thermocapillary convection increases. The

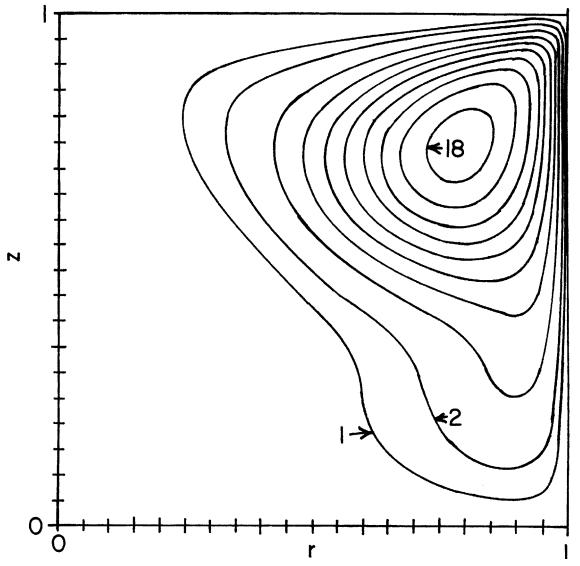

Fig. 5. Base-flow streamlines for $Pr = 0.02$, $Tm = 8000$ and $Re_{cr} = 4593$. $\psi_0 = 1$ and $\psi_0 = 2n$ for $n = 1$–9.

rapidly rising Re_{cr} for the propagating $m = 1$ mode eventually crosses the linearly increasing Re_{cr} for the convected $m = 2$ mode, resulting in the return to the latter mode as the critical instability. Wanschura et al. [5] used a perturbation energy balance to show that the key term driving the $m = 2$ instability is $v_{r1}\partial v_{z0}/\partial r$ in the axial perturbation momentum equation.

It appears that the effects of an RMF on the thermocapillary instability arise primarily from the azimuthal base-flow velocity $v_{\theta 0}$ produced by the RMF. An azimuthal base-flow velocity which is an even function of z can also be produced by rotating the crystal and feed rod at the same angular velocity and in the same azimuthal direction, which is generally called isorotation. The changes in the base-flow code are minor: $Tm = 0$ and $v_{\theta 0} = Re_\omega r$ at $z = \pm 1$, where $Re_\omega = \omega R^2/\nu$, and ω is now the angular velocity of the crystal and feed rod. There are no changes in the perturbation code. For $Pr = 0.02$, the values of Re_{cr} for both cases are plotted as functions of $v_{\theta 0max}$ for $0 < v_{\theta 0max} < 120$ in Fig. 6. For this range of $v_{\theta 0max}$, the effects of an RMF and of isorotation on the thermocapillary instability are very similar. As $v_{\theta 0max}$ increases from 120, the Re_{cr} for isorotation increases faster than that for an

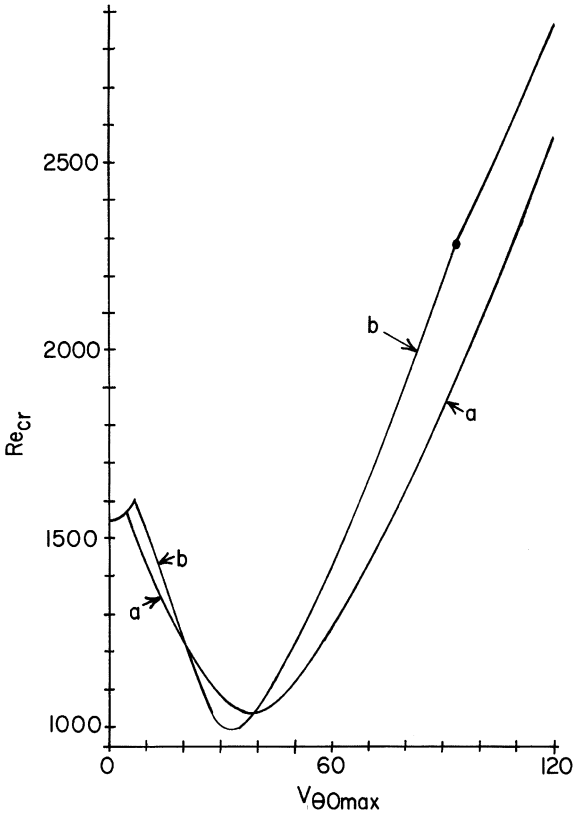

Fig. 6. Re_{cr} versus $v_{\theta 0max}$ for $Pr = 0.02$ and for: (a) a RMF, or (b) isorotation of the crystal and feed rod.

RMF. For example, at $v_{\theta 0max} = 180$, $Re_{cr} = 4112$ for an RMF and $Re_{cr} = 4819$ for isorotation, both for an antisymmetric, $m = 2$ mode. For a stronger RMF, the axial variation of the centrifugal force due to $v_{\theta 0}$ drives a meridional base-flow circulation which reinforces the thermocapillary convection, while isorotation at a large angular velocity leads to a small deviation from a rigid-body rotation, so that isorotation always damps the thermocapillary convection.

4. Conclusions

The thermocapillary instability in the FZ process without an RMF arises from the large radial gradient of the axial velocity near the free surface and leads to a steady, nonaxisymmetric flow. The addition of base-flow azimuthal velocity

by an RMF stabilizes this instability so that its Re_{cr} increases, and convects its nonaxisymmetric pattern with some mean of the base-flow angular velocity. As the strength of the RMF is first increased from zero, so that it adds a small azimuthal velocity to the strong meridional thermocapillary convection, a new instability arises from the interaction of the centrifugal force and the radial transport of angular momentum. For small values of Tm, this new propagating instability has a lower value of Re_{cr} than the basic convected thermocapillary instability. However, as the strength of the RMF increases and the base-flow centrifugal force becomes large enough to modify the meridional thermocapillary convection, this new instability is stabilized, leading to a rapid increase of its Re_{cr}, so that it eventually exceeds the more slowly increasing Re_{cr} for the convected basic thermocapillary instability, leading to a return to the latter as the first instability.

Dold et al. [2] presented experimental results for $Re = 74,000$–$223,000$ and $Tm = 9400$–$85,000$. For every experiment, the flow remained unsteady and nonaxisymmetric, but the cause of the residual deviation from axisymmetry may have been that the RMF was not strong enough to eliminate the hydrodynamic instability or it may have been the result of imperfections in the experiments. Clearly our range of values of Re_{cr} for $Tm = 0$–8000 does not correspond to their experiments. Nevertheless our results show that Re_{cr} for the convected $m = 2$ mode is increasing linearly with Tm for $Tm > 6000$. The linear extrapolation of our results leads to $Re_{cr} = 42,300$ at $Tm = 85,000$, which is far below the values of Re for their experiments. Of course, for $Tm > 8000$ another mode may become unstable before the convected $m = 2$ mode, but this would lead to a lower value of Re_{cr} after each mode switch. Therefore we conclude that the Re_{cr} for the first instability leading to transition from a steady, axisymmetric flow to a periodic, nonaxisymmetric flow is far below the values of Re in their experiments and that their RMF is not strong enough to eliminate the hydrodynamic instability.

Using the growth rate and the measured distances between adjacent maxima of the dopant concentration in the striations, Dold et al. [2] determined the frequencies of the unsteady melt motion for 14 mm diameter silicon crystals. For $Tm = 0$, they found a spectrum of frequencies which reflected a chaotic flow for their high value of Re, and which were concentrated below 1 Hz. For $Tm = 9400$, they again found a spectrum of frequencies, but with a shift to slightly higher frequencies. For $Tm = 21,000$, the spectrum of frequencies virtually disappeared, reflecting the elimination of chaotic flow, and there was a single strong frequency of 1.3 Hz. They stated that this single frequency correlated with the azimuthal velocity, indicating a single convected instability mode. For silicon with $R = 7$ mm, our characteristic time $R^2/\nu = 140$ s. For $Pr = 0.02$ and for the critical convected $m = 2$ mode, we found that $\lambda_I = 424.44$ for $Tm = 6000$ and $\lambda_I = 523.85$ for $Tm = 8000$. The results for(λ_I/m) for $m = 2$ in Fig. 2b indicate a linear variation of λ_I with Tm. Extrapolating our results for $Tm = 6000$ and 8000 to $Tm = 21000$ gives a frequency of 1.33 Hz. This good agreement between their experimental frequency and our extrapolated predicted frequency at $Tm = 21000$ may be a coincidence because the experimental Re is still well above the Re_{cr} for the first instability.

Acknowledgements

This research was supported by the US National Science Foundation under Grant CTS-0129028 and by the US National Aeronautics and Space Administration under Grants NAG 8-1453 and NAG 8-1705. The calculations were performed on a workstation donated by the International Business Machines Corporation.

References

[1] P. Dold, K.W. Benz, Prog. Cryst. Growth Characterization Mater. 38 (1–4) (1999) 7.
[2] P. Dold, A. Cröll, M. Lichtensteiger, Th. Kaiser, K.W. Benz, J. Crystal Growth 231 (2001) 95.
[3] H.C. Kuhlmann, H.J. Rath, J. Fluid Mech. 247 (1993) 247.
[4] H.C. Kuhlmann, M. Wanschura, V. Shevtsova, H.J. Rath, Adv. Space Res. 16 (7) (1995) 15.
[5] M. Wanschura, V.M. Shevtsova, H.C. Kuhlmann, H.J. Rath, Phys. Fluids 7 (5) (1995) 912.

[6] M. Levenstem, G. Amberg, J. Fluid Mech. 297 (1995) 357.
[7] R. Savino, R. Monti, Appl. Sci. Res. 56 (1996) 19.
[8] G. Chen, A. Lizée, B. Roux, J. Crystal Growth 180 (1997) 638.
[9] J. Leypoldt, H.C. Kuhlmann, H.J. Rath, J. Fluid Mech. 414 (2000) 285.
[10] G. Kasperski, A. Batoul, G. Labrosse, Phys. Fluids 12 (2000) 103.
[11] L. Martin Witkowski, J.S. Walker, P. Marty, Phys. Fluids 11 (7) (1999) 1821.
[12] B.T. Smith, et al., Matrix Eigensystem Routines—EISPACK Guide, 2nd Edition. Vol. 6 of Lecture Notes in Computer Science, Springer, New York, 1976.